International Journal of Thermofluids 27 (2025) 101275

Contents lists available at ScienceDirect

International Journal of Thermofluids

journal homepage: www.sciencedirect.com/journal/international-journal-of-thermofluids

CFD investigation of the shift of Nukiyama and Leidenfrost temperatures for high-pressure dense sprays hitting hot walls

Davide Viscione [a], Valerio Mariani [a,*], Stefania Falfari [a], Vittorio Ravaglioli [a], Giovanni Meccariello [b], Alessandro Montanaro [b]

[a] Alma Mater Studiorum – University of Bologna, Department of Industrial Engineering DIN, Bologna 40136, Italy
[b] Consiglio Nazionale delle Ricerche (CNR) – Istituto di Scienze e Tecnologie per l'Energia e la Mobilità Sostenibile (STEMS), Napoli 80125, Italy

ARTICLE INFO

Keywords:
Leidenfrost effect
Leidenfrost temperature shift
Nukiyama temperature shift
CHT spray simulation
Spray-wall impingement

ABSTRACT

In this paper the sensitivity of the Nukiyama and Leidenfrost effects to high velocity and high number density jets has been assessed. The effects of Nukiyama and Leidenfrost describe the non-linear and non-monotonous phase-change of liquid droplets upon a hot surface. According to fundamental experiments, these effects occur at two specific temperature values, i.e. the Nukiyama temperature and the Leidenfrost temperature. However, if dense jets are injected with high rate, the occurrence of these effects can be shifted at different temperatures values, mainly due to local thermos-kinetical effects produced by multiple hits of droplets at high frequency against the surface. In this work, this phenomenon has been investigated by means of three-dimensional computational fluid dynamics simulations of high-pressure fuel spray (300 bar - 700 bar) impinging a hot aluminium wall heated at different temperature values representative of the phase-change regimes. The surface temperature variation due to the spray impingement has been reproduced by means of the conjugate heat transfer approach, which relies on the coupling of the one-dimensional finite element method simulation of the surface. The methodology has been used to map the actual values of the Nukiyama and Leidenfrost temperatures and their shift compared to the reference experimental ones. The reasons behind the shift have been investigated by means of the three-dimensional results, then a correlation with the components of the average Weber number of the impinging droplets has been proposed.

1. Introduction

1.1. Framework

The wall impingement of liquid jets against hot surfaces is the focus of several studies, both experimental and numerical, because of its key importance in different technologies. If the surface temperature is higher than the saturation temperature of the impinging liquid, the liquid phase-change upon the surface features a complex evolution. The sequence of the phases faced by the liquid droplets upon a high temperature surface is exhaustively described by the so called 'droplet lifetime curve' [1] (Fig. 1). According to this curve, as the temperature of the surface increases above the saturation temperature of the liquid, three regimes can be distinguished:

- nucleate boiling: the droplet lifetime (i.e., the time frame during which the impinged substance adheres to the surface as a shaped liquid) decreases as the temperature increases up to a minimum value. This minimum is associated with the so-called Nukiyama temperature;
- transition boiling: the fast evaporation of the liquid leads to the formation of vapor zones which locally cool down the surface, resulting in a lower actual contact temperature between the solid and the non-evaporated liquid. In this regime, the droplet lifetime increases as the temperature increases above the Nukiyama temperature value. The droplet lifetime continues to increase up to a maximum value associated with the so-called Leidenfrost temperature. At the Leidenfrost temperature, the vapor zones have reached a consistent shape, resulting in the formation of a thin vapor film that fully prevents the contact between the solid and the non-evaporated liquid;
- film boiling: the droplet lifetime decreases as the temperature increases above the Leidenfrost value up to the complete change to vapor phase. In this regime, the super high temperature has

* Corresponding author.
E-mail address: valerio.mariani4@unibo.it (V. Mariani).

https://doi.org/10.1016/j.ijft.2025.101275

Available online 28 May 2025

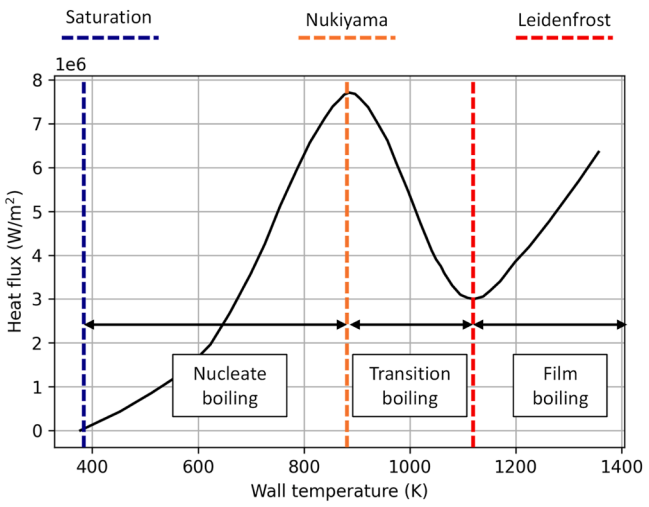

Fig. 1. Droplet boiling curve of Water. Data taken from [2].

destroyed the vapor film, leading to the lack of an insulating layer between the solid and the non-evaporated liquid.

In the field of droplet boiling curves reconstruction, a plethora of experimental works [3–8] present tests conducted under extremely controlled laboratory conditions. In these experiments the liquid droplets were gently dropped upon the surface by means of a needle, resulting in a limited velocity. Furthermore, the droplets were injected one by one, or with a regular pattern. These conditions pose two heavy limitations on the results obtained by the tests:

- Since the injection of liquids at high pressure is a common practice in the current state of technology, the gentle deposition of droplets is no longer representative of the phenomena occurring in real devices. Typically, the kinetic state of a droplet is well represented by the non-dimensional Weber number in Eq. (1), where ρ is the density of the liquid, σ is the surface tension of the liquid, D is the subscript associated to the liquid droplet, d is the droplet diameter, u is the relative velocity between the droplet and the back-gas. Using the component of the droplet velocity that is perpendicular to the surface ($u_\perp$), leads to the perpendicular Weber number ($We_\perp$), while using the component that is parallel to the surface ($u_\parallel$), leads to the parallel Weber number ($We_\parallel$). For the current typical spray injection pressure, the resulting values of the Weber number are thoroughly higher than those considered decades ago to draw up most of the spray-wall impingement maps [9–12]. It must be considered that droplets that feature a high Weber number are able to penetrate thin films of heavy hydrocarbons [13], thus, they would be able to slow down the formation of a thin film of vapor shifting, in fact, the occurrence of the Leidenfrost effect.

$$We_\perp = \frac{\rho_D\, d_D\, {u_\perp}^2}{\sigma_D}, \quad We_\parallel = \frac{\rho_D\, d_D\, {u_\parallel}^2}{\sigma_D} \tag{1}$$

- Since current sprays are very dense, their impingement against a surface leads to the spreading of large footprints that are complex in shape [14,15], while single droplets or lines of droplets lead to a contact point. Considering high surface temperature applications, the enhanced heat exchange induced by the footprint area may result in the shift of the occurrence of the Nukiyama and Leidenfrost effects.

Predicting the Nukiyama and Leidenfrost temperature values is a key requirement for different application areas: impingement of air-water jets against metal surfaces in atomized evaporative cooling techniques, urea-water liquid sprays for SCR (Selective Catalytic Reactors) in gas after-treatment devices, and fuel sprays in internal combustion engines.

In the framework of cooling techniques, e.g. continuous casting and thermal treatments of metal surfaces, the use of air jets enriched with dispersed water droplets is an effective method to enhance the heat exchange coefficient by using the droplet phase change upon the hot surface [16]. The effectiveness of the cooldown provided by the water spray setup is crucial in order to ensure the target solid structure, and its mechanical properties. If the Leidenfrost effect occurs unexpectedly, a thin film of water vapor covers the hot surface of the metal piece, strongly reducing the heat exchange coefficient. As a result, the effectiveness of the cooling technique may be limited for dozens or hundreds of seconds [17] because the Leidenfrost vapor film is a structure that is slowly consumed. In [18] Hnizdil et al., based on their optical experimental measures, report that the Leidenfrost effect may occur from 423 K to 1273 K depending on the spray features. The authors propose a correlation that returns the shift of the Leidenfrost temperature depending on the water spray density upon the contact surface, the droplet velocity and the droplet Sauter mean diameter.

SCR devices are components of the aftertreatment system in the balance of plant of internal combustion engines, aimed at reducing the concentration of nitrogen oxides at the tailpipe. SCRs can be installed both on traditional Diesel engines as well as on the next generation of spark ignition engines, which should work with lean and ultra lean mixtures, e.g. engines fueled with hydrogen, natural gas and biogas for power generation or maritime transportation. A solution of water and urea is injected in the form of liquid spray before the SCR, so that the combination of the high temperature of the back-gas (i.e., the engine exhaust gases), and that of the exhaust pipe itself, promotes the evaporation and the thermal decomposition of the injected solution into ammonia [19]. The understanding of the influence of the phase-change thermal regimes faced by urea-water droplets upon the exhaust pipe surface is mandatory in order to assess the SCR conversion efficiency, and the possible occurrence of ammonia slip. Even though the typical injection pressure of urea-water jets is relatively low (5–10 bar), the short distance between the free jet and the walls may lead to impinging droplets at 25–30 m/s, namely Weber number values over 150. The identification of the Leidenfrost effect under SCR conditions, and the evaporation time of impinged urea-water droplets have been experimentally studied in recent works [20–22] without any focus on the shift of the phenomena due to real spray dynamics. In [23,24], the authors present experimental data that show the upward shift of the Leidenfrost temperature due to the porosity of the surface material, which speeds up the consumption of the vapor layer, since vapor can escape the surface through the pores.

In direct injection internal combustion engines, at high load especially, the fuel spray impinges the hot surface of the piston head, resulting in the split of the impinged fuel mass into fuel film and reflected droplets. The piston temperature strongly affects both the mass split ratio, and the characteristics of the reflected spray, thus influencing the local distribution of the fuel vapor in the oxidizer. To reduce the harmful emissions of engines, the repeatability of the mixture formation is compulsory. To this aim, the optimal design of the fuel spray targeting has gained increasing attention in the last decade. It is highlighted that in modern engines based on low temperature combustion concepts, the timing of the main injection event (i.e., the one that mainly contributes to the torque) is usually positioned near the top dead center, when the piston is very close to the injector tip. In this condition, the distance between the free jet and the surface is extremely short. Moreover, the impingement of such dense and high velocity spray on the hot surface results in a significant local cool-down of the piston [25]. These colder spots may act as sources of soot formation, since successive droplets would face a lower surface temperature. The next generation of engines will rely on both advanced injection technologies (injection pressure up to 700 bar), and new net-zero emissions e-fuels, whose thermophysical

behavior under engine conditions must be characterized. In this framework, mapping the shift of the Nukiyama and Leidenfrost effects is important to achieve a comprehensive understanding of the fuel spray injection setup.

1.2. Contribution

To the best knowledge of the authors, poor attention has been posed on the shift of the Nukiyama and Leidenfrost effects induced by jets with high velocity and high number density. Something on this research topic has been presented by Hnizdil et al., [18] with focus was on optical Particle Image Velocimetry (PIV) methods for water atomization. However, it is underlined that optical facilities equipped with PIV are expensive, uncommon, and require a very specific competence. Therefore, reproducing that setup to determine new correlations to predict the shift phenomenon for different fluids and applications would not be viable. Computational three-dimensional simulations can be attractive in order to collect hints on the boiling regimes faced by the liquid under real jet conditions. In several simulation software there are two different options to set the Nukiyama and Leidenfrost temperatures i.e. setting fixed values or choosing between different models based on the critical properties of the fluid [26] and on the back pressure of the vessel [27,28]. However, heavily dense and fast sprays can shift the occurrence of the Leidenfrost effect towards temperature values that are different from the theoretical one. Having hints on the shift of the Nukiyama and Leidenfrost temperature values for real conditions can support the optimization of the spray targeting, the injector positioning and the properties of the liquid phase at given injection pressure and wall temperature.

It is also underlined that in [18] the authors correlate the Leidenfrost temperature of a real jet with the volume flow rate per unit surface, the droplet velocity and the Sauter mean diameter. However, the volume flow rate per unit area used as a parameter in their correlation can be hard to estimate, because it strongly depends on the local incident of the jet. In order to improve the feasibility of the correlation, non-dimensional quantities and some key operating conditions can be used as parameters. Moreover, the correlation proposed in [18] bonds the chosen parameters directly with the effective Leidenfrost temperature, without any explicit dependence from the liquid properties. This limits the use of their correlation to jets made of water. We believe that the validity of this analysis can be extended by identifying a correlation for the shift of the Leidenfrost temperature which must be then added to its reference values, that is calculated based on the adopted liquid.

In light of the above, this work deals with the CFD (Computational Fluid Dynamics) three-dimensional simulation of liquid sprays injected at high pressure against a heated wall. The dynamic thermal phenomena faced by the droplets upon the wall have been simulated by coupling the CFD simulation with a one-dimensional Finite Element Method (FEM) solver. CFD and FEM solutions are coupled by the heat flux equation. The simulation tests presented in this work are the same chosen in a previous experimental work of the same authors [29] in the field of internal combustion engine. The resulting effective boiling curves show that the regime switch (from transition boiling to film boiling) occurs within a tighten range of wall temperature compared to the ones based on theory. Eventually, the shift of the Leidenfrost temperatures has been correlated both with the average Weber number of the spray and with the operating parameters (injection pressure, distance).

2. Methodology

The simulation domain and the simulation matrix as well are consistent with the experiments conducted by the same authors [29] in an optically accessible vessel which features a smooth aluminum wall at the bottom. The temperature of the wall was controlled electrically by a J-type thin thermocouple located at the center 1.0 mm under the surface. The impinging jet was commercial pump gasoline at 298 K (Table 1) injected by means of a single-hole common-rail diesel injector (100 μm in diameter) installed at the top of the vessel.

Table 1
Main properties of the tested fuel.

Fuel property	Pump gasoline
Density @15 °C (kg/L)	0.720–0.775
Vapor pressure @38 °C (kPa)	48–103
Specific heat (kJ/kg/K)	2
Viscosity @20 °C (mPa s)	0.37–0.44
Lower heating value (MJ/L)	30–33

2.1. CFD model setting

The software used to run the CFD simulations is STAR-CD by Siemens. The computational domain is a box of 80 mm width x 80 mm length, while the height depends on the tested distance between the injector tip and the wall. The grid base size was set to 4 mm in the regions in which the presence of fuel droplets is not expected according to the experimental measurements [29]. The spray region was meshed by using a base grid size of 1 mm with two refinements around the injection point realized in order to capture the spray atomization and breakup. As a result, the cell size was fined up to 0.5 mm along 10 mm downstream the injector tip, and then up to 0.25 mm along 5 mm.

The transport equations based on the Reynolds-Averaged Navier Stokes (RANS) approach were discretized using a second-order central differencing scheme and a fixed time step of 0.5 μs. The two-equations $k-\varepsilon$ RNG model was adopted to account for the turbulence. The evolution of the spray was captured in a Lagrangian manner: the Huh and Gosman model [30] was used to simulate the atomization, and the Reitz and Diwakar model [31] was used to simulate the secondary break-up. During the breakup process, the mutual interaction between computational droplets was enabled by using the O'Rourke model [32]. As a wall-impingement model, the STAR-CD custom Bai-ONERA model [9,10] was chosen. The setup of the atomization model, the breakup model, and the wall-impingement model was successfully validated against experimental data in previous works of the present authors [29,33] on the same topic.

Determining the Nukiyama (T_N) and Leidenfrost (T_L) temperature values is crucial to reproduce the heat transfer between the generated liquid fuel film and the heated wall. According to the Bai-ONERA model, the thermal regimes that a droplet upon a surface may face are described by the non-dimensional temperature T^* defined as the Eq. (2), where T_w represents the temperature of the wall:

$$T^* = \frac{T_w - T_N}{T_L - T_N} \tag{2}$$

For $T^* < 0$, the wall temperature is lower than the Nukiyama one, this condition represents the nucleate boiling regime. The condition $0 < T^* < 1$ represents *the transition boiling r*egime. For $T^* > 1$, the wall temperature is greater than the Leidenfrost one, this condition represents the film boiling regime. Since the tested room pressure is the atmospheric pressure, the reference Leidenfrost temperature was calculated by using the correlation proposed by Spiegler [26] (Eq. (3), where T_c represents the critical temperature).

$$T_L = \frac{27}{32} T_c \tag{3}$$

In this study, a pseudo-pure liquid named Gasoline1 was selected from the STAR-CD database. This fluid mimics the main characteristics of the commercial gasoline. In particular, the critical temperature is 544 K, thus, the Leidenfrost temperature at 1 bar ($T_{L,1bar}$) is 459 K. In order to identify the Nukiyama temperature, the midpoint approach [28,34] was used (Eq. (4), where $T_{s,1bar}$ is the normal boiling temperature of the Gasoline1, namely 371 K). As a result, the Nukiyama temperature was

set at 415 K.

$$T_{N,\ 1\ bar} = \frac{T_{s,1\ bar} + T_{L,1\ bar}}{2} \tag{4}$$

2.2. CHT model setting

During the setup of the boundary conditions of the CFD simulation, the software enables the use of an additional module called Conjugate Heat Transfer (CHT) that calculates the temperature of the wall iteratively at each time-step based on the fluid phenomena occurring upon the wall. Therefore, the CFD three-dimensional simulation is coupled with a one-dimensional FEM model (Fig. 2) that computes the temperature variation along the thickness of the solid wall caused by the conduction across the solid, and by the convection upon the surface (Fluid-Solid Interface (FSI)). The CHT module requires the thermophysical properties of the solid material (Table 2), and the bulk thickness i.e., the depth from the FSI at which the temperature is not affected by the heat transfer. In order to run the FEM simulation, an arbitrary number of solid layers of heigh δ must be placed below the FSI.

Preliminary simulations were conducted to test the influence of the number of layers and of the bulk on the results. Fig. 3 reports the behaviour of the temperature at the FSI for different number of layers considering the wall temperature of 423 K. Since the CHT model is applied to the whole boundary, the average variation compared to the initial temperature is limited, being the spray-wall impingement focused in a relatively small zone of the wall. As visible in Fig. 3, for a number of layers higher than ten, the resulting wall temperature profiles are almost overlap, thus, a value of 100 layers was chosen.

3. Results

In this section, we discuss the results obtained with the CFD simulations on the test points listed in Table 3. These points were chosen because they are representative of the injection conditions and timing in a reference low temperature combustion engine. It is underlined that the spray-wall impingement methodology proposed in this work was validated on these points against experimental data in [29]. In order to record the cooldown of the wall due to the impingement of the spray, the CFD boundary results were processed with a *Matlab* algorithm able to select only the faces of the cells with a temperature value different from the initial one. The temperature values of this subset of cells were then averaged to determine the mean temperature that was used to calculate the local cooldown of the wall as in Eq. (5). Fig. 4 shows the temperature of each cell face on the FSI selected by the algorithm for the results analysis.

$$\Delta T(t) = T_w(t) - T_w(0) \tag{5}$$

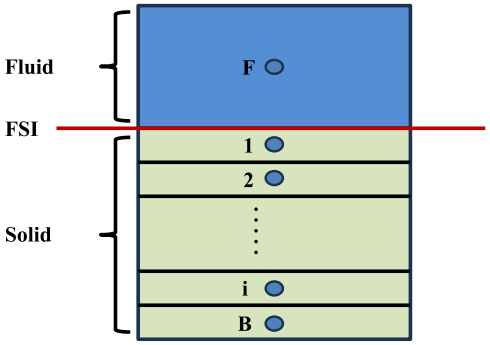

Fig. 2. Schematic of the implemented conjugate heat transfer approach.

Table 2
Properties of the metal surface used for wall impingement tests.

Thickness (mm)	1
Density (kg/m^3)	2698
Thermal conductivity (W/m/K)	210
Specific heat (J/kg/K)	900
Roughness (μm)	1

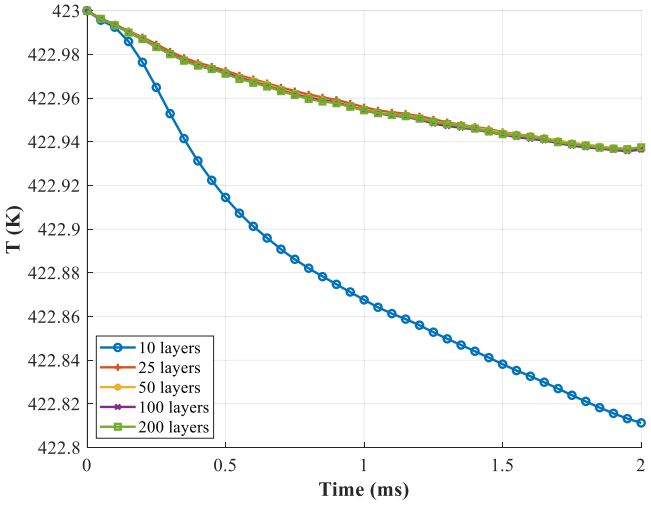

Fig. 3. Surface temperature profile for different number of layers.

Table 3
List of the simulation campaign points.

Distance (mm)	Injection pressure (bar)	Surface temperature (K)
20	500	298 – 415 – 493
	700	
30	500	
	700	

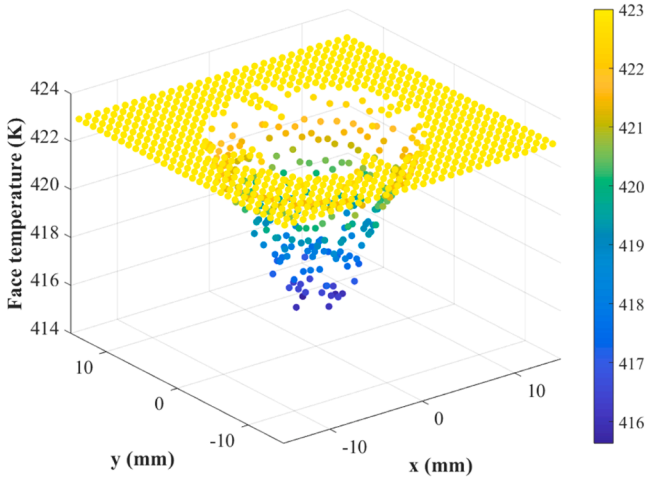

Fig. 4. Temperature of the cells faces of the surface at 2 ms after start of injection. Test 423 K, 20 mm, 700 bar.

3.1. Sensitivity to the Nukiyama temperature definition

In this section, the sensitivity of the heat exchanged to the Nukiyama temperature calculation method is presented. At given saturation temperature and Leidenfrost temperature, it is important to evaluate the

robustness of the midpoint approach (Eq. (4)) adopted for the identification of the Nukiyama temperature. From experimental data in the literature [3–8], it is known that for pure hydrocarbons the ratio between the Nukiyama temperature, and the saturation temperature is in the range 1.05 (for n-hexane) – 1.2 (for n-dodecane). Since pump gasoline is mainly made of hydrocarbons with carbon number between C5 and C9, the sensitivity test has been conducted by performing a sweep of the Nukiyama temperature value including that of n-hexane ($1.05 \cdot T_{s,1bar} = 389$ K) and that of n-dodecane ($1.2 \cdot T_{s,1bar} = 445$ K) as extrema, as well as the one returned by the use of the midpoint approach (415 K). For this test, the initial wall temperature has been set at 423 K, chosen in order to fall in the transition boiling regime ($0 < T^* < 1$). Table 4 lists the different conditions adopted for the following tests.

Fig. 5 shows the behaviour of the wall temperature and that of the wall heat flux for the three Nukiyama temperatures values listed above. The test with the value 389 K shows a delayed cooling effect during the early injection. Instead, the tests with the values 415 K and 445 K have almost the same evolution of both wall temperature and heat flux. Considering the overlap between the curves associated with a Nukiyama/saturation ratio between 1.1 and 1.2, and that the phase-change properties of commercial gasoline are well represented by C8 components, the midpoint rule has been considered reliable.

3.2. Assessment of the surface cooldown

Consistently with the theory behind the Nukiyama effect, the maximum heat flux, thus, the maximum cooldown of the wall, occurs when $0 < T^* < 1$ (transition boiling regime). Since the Nukiyama temperature value has been set at 415 K, the simulation tests characterized by the wall temperature 423 K have a non-dimensional temperature $T^* = 0.18$, thus, the maximum heat flux is expected. The simulation tests characterized by the wall temperature 493 K have a wall temperature above the Leidenfrost temperature (459 K), and a non-dimensional temperature $T^* = 1.77$ (film boiling regime). In these cases, a limited cooldown of the wall should be expected, since the fuel vapour layer insulates the liquid film from the wall, leading to a reduced heat flux. In the simulation tests characterized by the wall temperature 298 K, no wall temperature variation is expected ($T^* = -2.66$), since the liquid film and the wall are in thermal equilibrium.

Fig. 6 shows the wall temperature variation for the three tested temperatures (298 K, 415 K, 493 K) at different values of the injection pressure (columns in Fig. 6) and at a different distance between the injector and the wall (rows in Fig. 6). As expected, the average cooldown around the spray impingement zone is zero for the test at 298 K (nucleate boiling regime, blue lines), whilst a slight temperature reduction (< 0.5 K) can be observed for the test at 493 K (film boiling regime, yellow lines). These two temperature tests show almost the same behaviour at any injection pressure and distance. The tests at 415 K (transition boiling regime, red lines) show a moderate average cooldown (around 3.5 K). During the early spray-wall impingement (time < 0.25 ms after the start of injection) the temperature reduction is quite steep due to the high exchange surface created by the spreading of the liquid fuel footprint, and the enhanced heat exchange driven by the phase change. Moving towards advanced instants, the new impinging droplets stack on the previously formed footprint, promoting the increasing of the thickness and of the thermal inertia of the wall film and not the exchange area. As a result, the longer is the record time after the start of injection, the more the temperature variation curve is flat.

Focusing on the effect of the injection pressure, it is underlined that the same energizing time has been applied for both the injection pressure values, thus, during the simulation tests conducted at 700 bar, the injector shoots a larger amount of fuel mass against the wall compared to that injected at 500 bar. At a higher injection pressure the spray breakup is enhanced, leading to larger number of parcels that can impinge the wall in different positions. Therefore, the higher is the injection pressure, the larger are the spray footprints, and the heat flux as well. Focusing on the effect of the distance between the injector and the wall, it is worth to mention the non-monotonous decreasing profile of the cooldown under transition boiling conditions. In Fig. 6 it is visible that for advanced instants after the start of injection, the wall temperature reduction has a maximum, then, the wall heats up. This is observed because the longer distance promotes the liquid fuel mass transformation from dispersed to vapour, thus, a smaller mass is available to form the wall film. As a result, the spray footprints are thinner, and they can evaporate faster. It is underlined that the position of the maximum temperature reduction at 700 bar, is more advanced compared to that recorded at 500 bar because of the greater spray momentum at higher injection pressure, which produces a deeper penetration across the fuel film.

3.3. Analysis of the fuel mass split

In this section, the analysis of the injected mass split into liquid film, dispersed droplets, and vapour is presented. This analysis can confirm the boiling regime in which the tested points fall, e.g. the lack of wall film mass and a significant mass of droplets at the same temperature are sign of the transition to the film boiling regime. More, a significant increase of the vapour mass and a moderate mass of wall film at the same temperature, are a sign of the switch to the transition boiling regime. Fig. 7 (20 mm distance) and Fig. 8 (30 mm distance) show the curves of the fuel mass percentage in the form of wall film (blue), dispersed droplets (red), vapor (green) together with the profile of the total actual injected liquid (black). The results are shown for both the tested injection pressure values i.e., 500 bar (left column) and 700 bar (right column).

In Fig. 7 and Fig. 8 it is visible that the maximum wall film mass is created for the wall temperature 298 K, i.e. when the nucleate boiling regime is expected. As shown Figs. 7a1–7a2, at 2 ms after the injection start, the 40 % (700 bar) - 50 % (500 bar) of the total injected liquid mass remains upon the wall as wall film. At the end of the test, the 65 % (700 bar) - 80 % (500 bar) of the total injected liquid mass is in the liquid phase (as wall film or dispersed droplets). The left mass percentage is in the vapor phase, mainly created due to the break-up phenomena. This can be confirmed by the lower mass percentage in the liquid phase recorded at 30 mm distance and 298 K (Figs. 8a1–8a2), compared to that recorded at 20 mm distance at the same wall temperature (Figs. 7a1–7a2).

Focusing on the simulations at high wall temperature (Figs. 7b1–7b2, 7c1–7c2 and Figs. 8b1–8b2, 8c1–8c2), the injected mass split is quite different compared to the case at 298 K. The tests in which the transition boiling regime is expected (Figs. 7b1–7b2, Figs. 8b1–8b2) present the minimum values and the flatter profile of dispersed mass. This is consistent with the onset of the Nukiyama effect, in fact, the droplets heavily evaporate upon the wall and converted into vapour. In

Table 4
List of the test Nukiyama temperatures.

Distance (mm)	Injection pressure (bar)	Surface temperature (K)	Nukiyama temperature (K)	Saturation temperature (K)	Leidenfrost temperature (K)
20	700	423	389 415 445	371	459

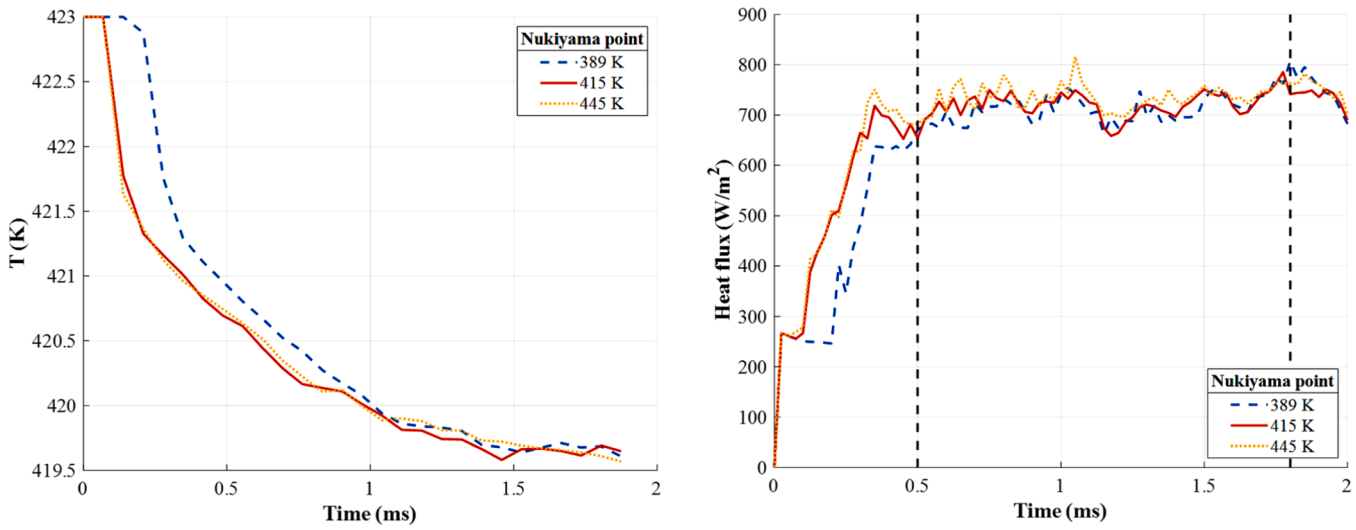

Fig. 5. Evolution of the surface temperature and the heat flux for three different Nukiyama temperature values.

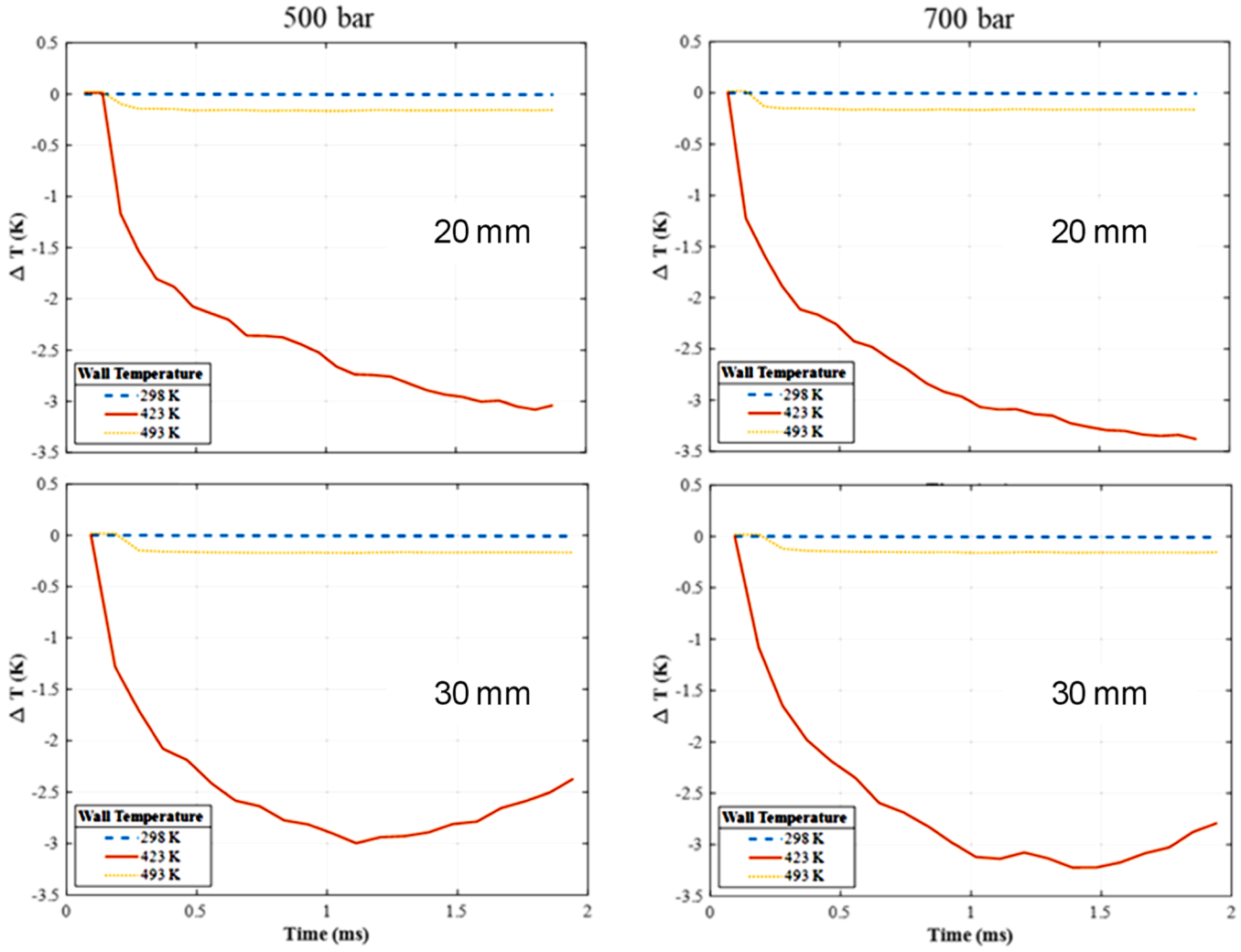

Fig. 6. Cooldown of the surface around the spray area at the injection pressure 500 bar (left) and 700 bar (right), 20 mm and 30 mm downstream the nozzle tip.

the tests in which the film boiling regime is expected (Figs. 7c1–7c2, Figs. 8c1–8c2) no liquid film is created (0 % wall film mass), the total injected liquid mass is only split into dispersed droplets and vapour in line with the onset of the Leidenfrost effect. The large percentage of liquid mass converted in vapor upon the wall (60 % to 80 % depending on the case) reduces the cooldown of the wall since the heat can only be

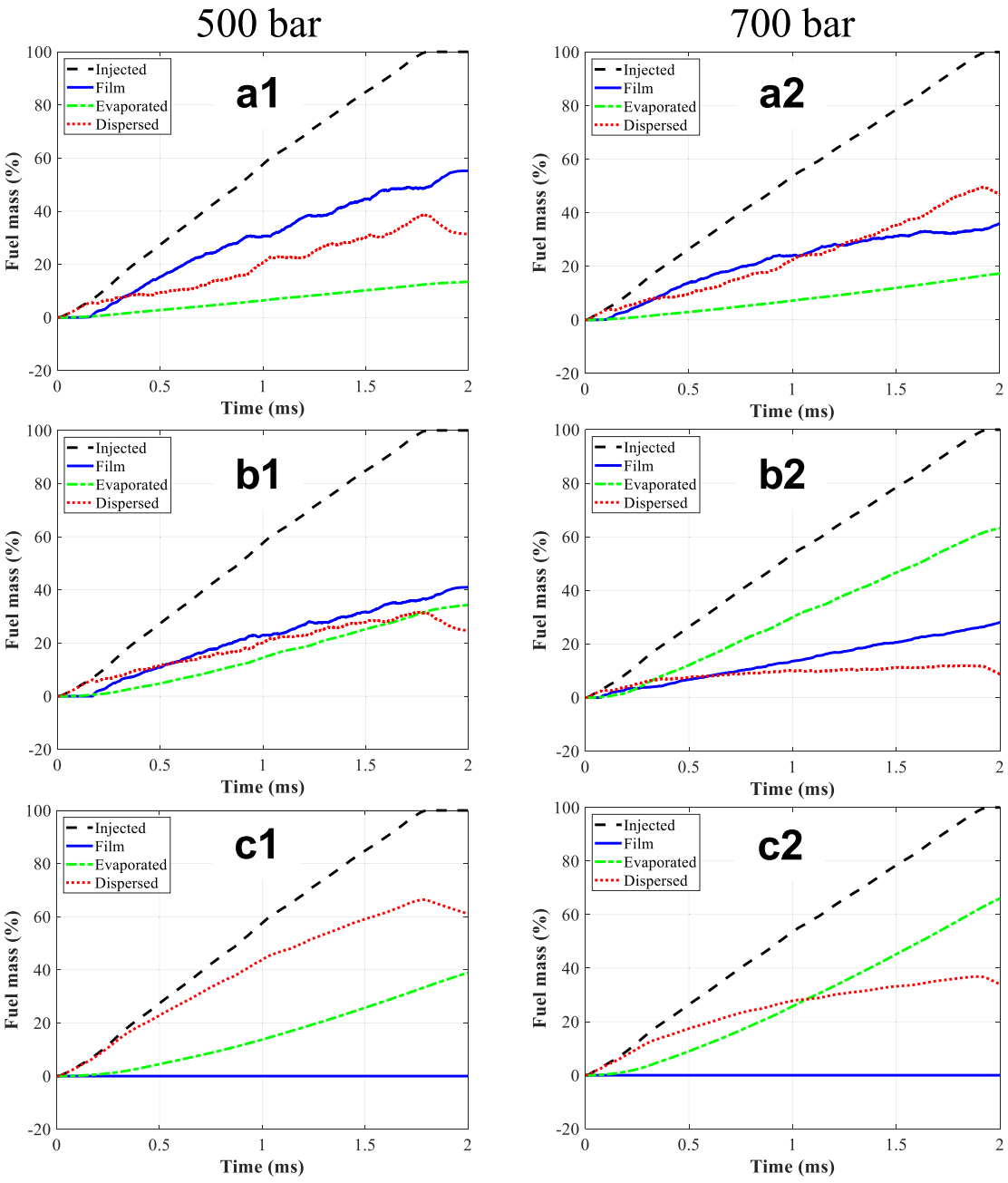

Fig. 7. Evolution of the injected mass, evaporated mass, dispersed mass and film mass at 500 bar (left) and 700 bar (right), and distance 20 mm. Wall temperature at 298 K (a1, a2), 415 K (b1, b2), 493 K (c1, c2).

exchanged by convection, confirming the observation reported in Fig. 6.

3.4. 4 analysis of the boiling curves

The main aim of this study is to draw up the droplet boiling curves (coordinates wall temperature – wall heat flux) of a gasoline-like fuel under realistic spray wall-impingement conditions, discussing the role of realistic spray velocity and number density on the results. In order to increase the discretization of the curves along the wall temperature axis, new CFD simulations with different wall temperature values have been added to the initial set of three values (289 K, 415 K, 493 K). For each simulation, the heat flux is returned by the CFD software for each cell face on the bottom boundary and then averaged across the whole surface. Furthermore, in order to determine a pattern for the effect of the injection pressure, the set of simulations (20 mm and 30 mm distance, wall temperature from 389 K to 500 K) has been repeated setting the injection pressure at 300 bar. The boiling curves are shown in Fig. 9 for the three injection pressure values 700 bar (yellow), 500 bar (red), 300 bar (blue). For the sake of comparison, the reference Nukiyama and Leidenfrost temperature values calculated by means of Eq.s 4, 3 are also shown.

In general, it is visible that the higher is the injection pressure, the higher are the Nukiyama and Leidenfrost temperature values. This thermal effect depends on the higher number density and the smaller diameter of the droplets induced by the higher injection pressure before the impingement (Fig. 10, 11) due to the enhanced breakup. Because of the higher number density and smaller droplets, the wall is hit with a higher frequency in multiple points, slowing down the formation of vapor structures, and the occurrence of the Nukiyama temperature as well. On the other hand, at higher wall temperature, the higher number

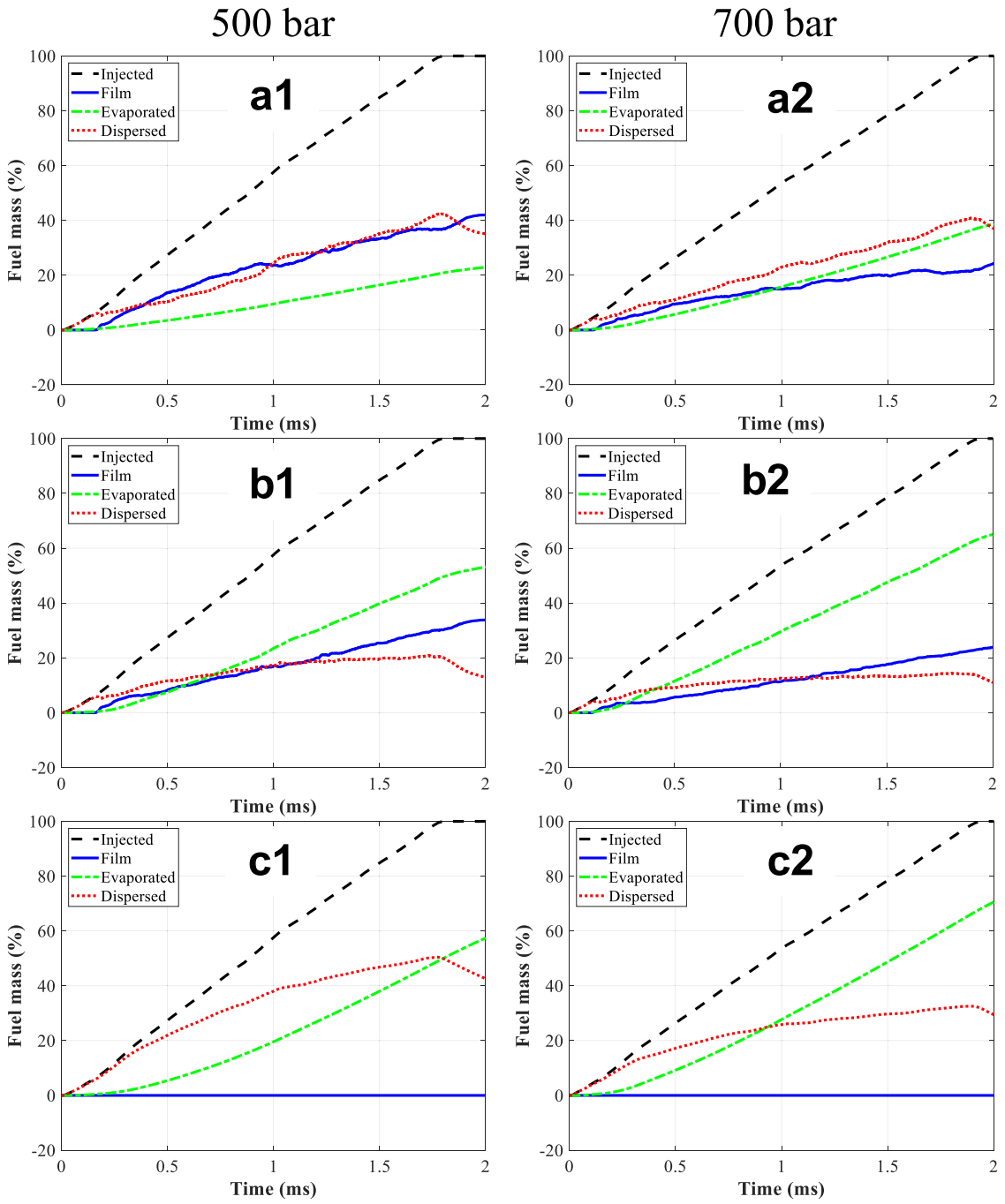

Fig. 8. Evolution of the injected mass, evaporated mass, dispersed mass and film mass at 500 bar (left) and 700 bar (right), and distance 30 mm. Wall temperature at 298 K (a1, a2), 415 K (b1, b2), 493 K (c1, c2).

density and smaller diameter produced by higher pressure values increase the ability of the droplets to hit the vapor layer, thus, to reduce its consistency. This leads to the slowing down of the occurrence of the Leidenfrost effect.

It is visible that both the maximum heat flux, corresponding to the effective Nukiyama temperature, and the minimum heat flux, corresponding to the effective Leidenfrost temperature, are not in line with the two reference lines. In Fig. 9, for each injection pressure the wall temperature at which the maximum heat flux is recorded is higher than the one calculated with the midpoint rule.

The actual wall temperature at the minimum heat flux lies around 425 K - 465 K, thus, with a difference between 10 K-50 K compared to the reference value (415 K). This difference is in line with the one reported in other studies [35,36]. On the other hand, the minimum heat flux, where the Leidenfrost effect occurs, is mainly recorded at lower wall temperature values compared to the reference one. To deeply investigate this behaviour, the two components of the Weber number (perpendicular $We_{\perp}$ and parallel $We_{\parallel}$, Eq. (1)) have been involved in drawing the maps of the shift of the Leidenfrost temperature (Fig. 12). The six markers in the map represent the minimum points of the six droplet boiling curves shown in Fig. 9, and the map is the fitting surface of these points. The shift of the Leidenfrost temperature has been calculated as the difference between the effective Leidenfrost temperature recorded (i.e., the temperature at which the heat flux is minimum) and the reference Leidenfrost temperature calculated by means of Eq. (3).

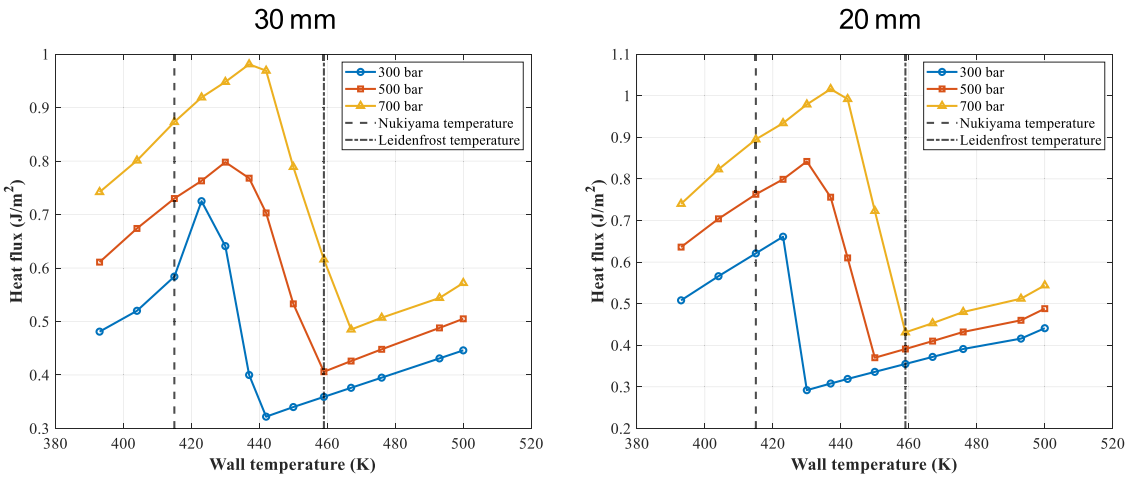

Fig. 9. Droplet boiling curves for different injection pressure values at 30 mm and 20 mm between the injector and the surface.

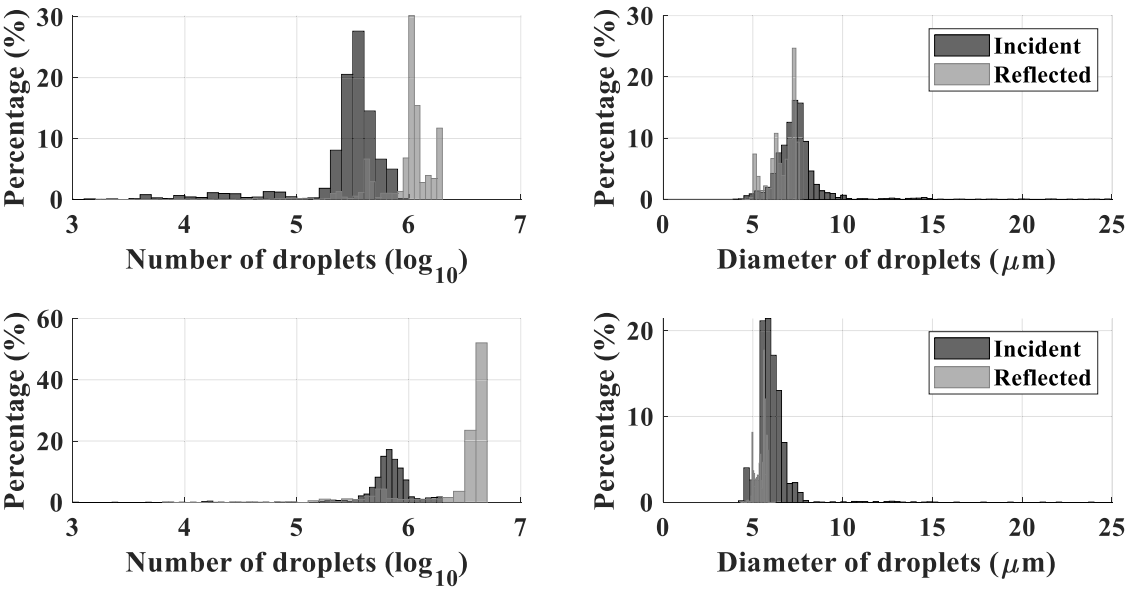

Fig. 10. Distribution of number and diameter of the droplets, both incident (dark grey bars) and reflected (light grey bars) at 20 mm distance for different injection pressure values.

From Fig. 12, the following points can be summarised:

- Focusing on point 1 and point 2, it is visible the effect of increasing the perpendicular Weber at given parallel Weber. The points are from the case at lower injection pressure (300 bar) and different distance (20 mm and 30 mm, respectively). At relatively low injection pressure, the higher is the perpendicular Weber, the more the Leidenfrost temperature is shifted backward. This is caused by the higher rate of vaporization induced by high perpendicular Weber component because of the higher rate of impact. Besides, the higher is the perpendicular Weber number, the higher is the kinetic energy along the perpendicular direction. At the wall impingement, this high kinetic energy is transferred as deformation energy of the liquid surface which promotes a strong flattening of the droplet. The latter phenomenon is responsible of dense, high surface and low thickness footprints. It is worth to mention that this behaviour is not monotonous; in fact, it features a bell shape if the perpendicular Weber would have been increased further ($We_\perp > 1600$, e.g. in the case of injection pressure);
- Focusing on point 2 and point 3, it is visible the effect of increasing the parallel Weber at given perpendicular Weber. The points are from the case at lower distance (20 mm) and different injection pressure (300 bar and 500 bar, respectively). The higher is the parallel Weber, the shorter is the backward shift of the Leidenfrost temperature. This is caused by the combination of the larger spreading of the footprint promoted by the higher parallel component, and the lower kinetic energy along the perpendicular component. Indeed, at the wall impingement, the droplet kinetic energy along the parallel component is transferred as shear deformation energy, promoting high thickness and sparse footprints.
- Focusing on point 1, point 3, and point 5 it visible the effect of a balanced split between perpendicular and parallel components, while increasing the overall Weber number of the impinging droplet $\left(We = \sqrt{We_\perp{}^2 + We_\parallel{}^2}\right)$, thus, increasing the overall momentum. Moving from point 1 towards point 5, the Leidenfrost effect is progressively retarded. At point 5, the shift of the Leidenfrost temperature compared to the reference one changes in sign, resulting in an upward shift. The same behaviour is visible moving from point 5 to point 6 and from point 5 to point 4. Thus, regardless to the split of the kinetic energy between parallel and perpendicular component, a very high overall Weber number leads to the upward shift of the

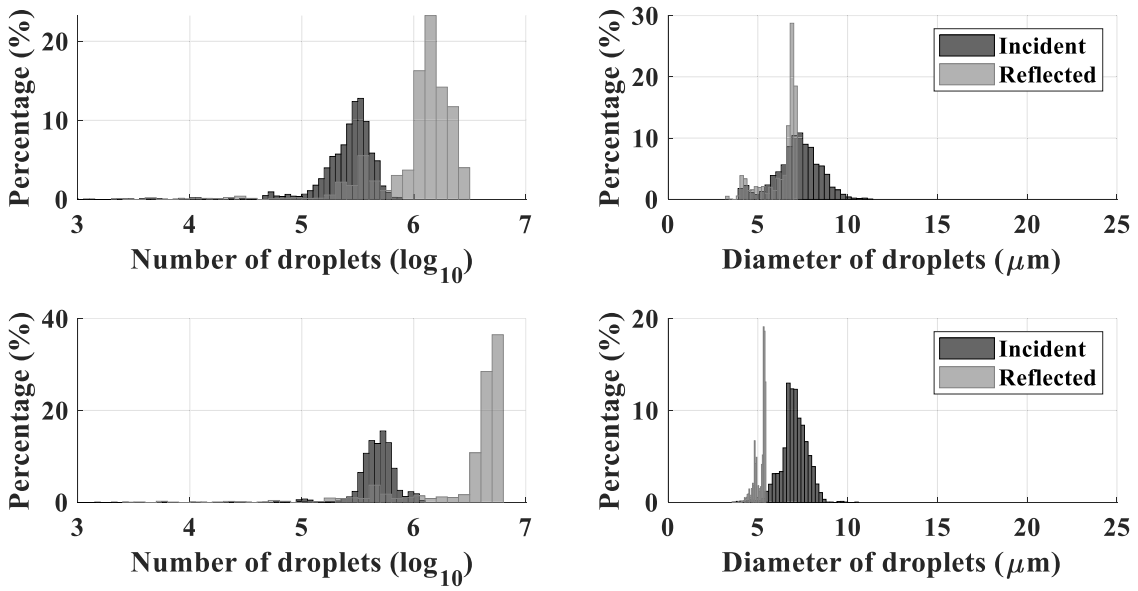

Fig. 11. Distribution of number and diameter of the droplets, both incident (dark grey bars) and reflected (light grey bars) at 30 mm distance for different injection pressure values.

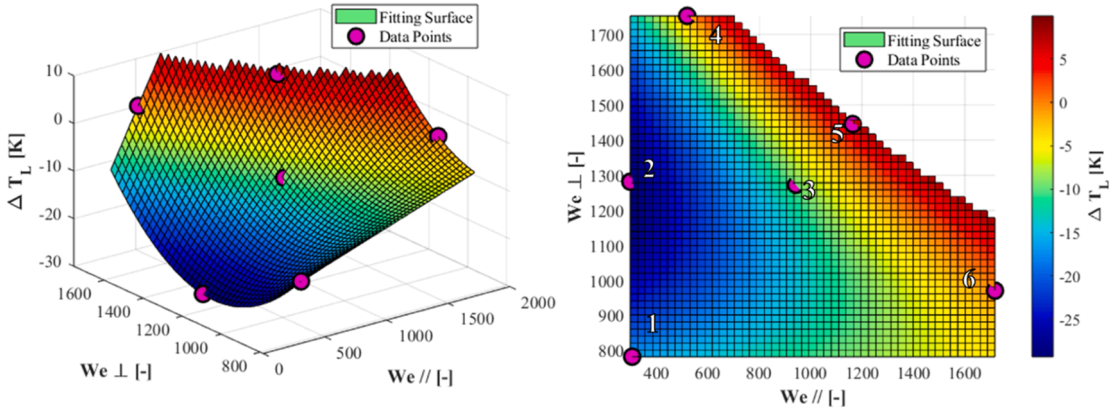

Fig. 12. Maps of the Leidenfrost temperature variation depending on parallel and perpendicular components of the Weber number.

Leidenfrost effect compared to the expectations. Aside from the distribution of the kinetic energy along the parallel and the perpendicular direction, droplets with an overall Weber number higher than a threshold value, are able to penetrate the forthcoming vapor layer and countering its formation. In this study, the threshold resulting from the analysis of the map is around $We > 1800$.

The insights deduced from the map can be summarized by the correlation reported in Eq. (6). The shift of the reference Leidenfrost temperature features a quadratic dependence from the perpendicular Weber number, and a linear dependence from the parallel Weber number. Due to the quadratic dependence, if the spray-wall setup promotes the distribution of the kinetic energy along the perpendicular direction, the delay Leidenfrost effect may occur easily (e.g. for lower injection pressure). Given a value of the perpendicular Weber number (e.g., $We_{\perp} = 1200$), the magnitude of the parallel component needed to delay the Leidenfrost effect is significantly higher than the magnitude of the perpendicular component needed if the same value is given for the parallel one (i.e., $We_{\parallel} = 1200$).

$$\Delta T_L = 72.81 - 0.0268 We_{\parallel} - 0.1672 We_{\perp} + 0.0001 We_{\perp}^2 \quad (6)$$

It is expected that the validity of Eq. (6) can be extended to injection pressure values and distance values above and below the range investigated in this work. Besides, considering that the values of the liquid density and of the surface tension of hydrocarbons lie in a relatively narrow range, it is expected that Eq. (6) can fit the response of other gasoline blends and e-fuels with slight modifications to the values of the constants. On the other hand, the validity of Eq. (6) is not ensured for walls with irregular surfaces e.g. n-curved surfaces and free forms because of the complexity to define the two components of the Weber number locally depending on the impingement point.

In Fig. 13 the shift of the Leidenfrost temperature is mapped on the chosen operating conditions as coordinates, i.e. injection pressure and distance. The shape of the fitting surface is expressed in Eq. (7), which describes the linear dependence from the distance, the quadratic dependent from the injection pressure, and the cross dependence from the two conditions. Fig. 13 shows that for any injection pressure, the higher is the distance, the more the anticipation of the Leidenfrost effect is reduced. As seen in Figs. 10 and 11, increased distance values cause reduced velocity and diameter of the droplets due to the longer effect of the breakup phenomenon. As a result, the higher is the distance, the lower will be both the impingement rate and the evaporation rate at the wall, namely the formation of the insulating vapor layer will be slowed down.

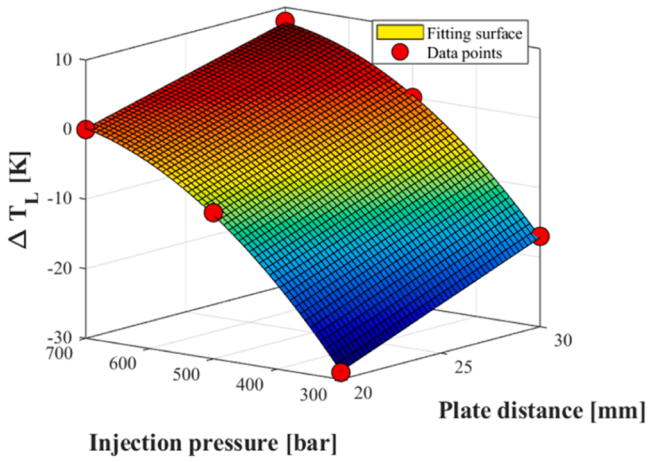

Fig. 13. Maps of the Leidenfrost temperature variation depending on injection pressure and distance.

$$\Delta T_L = -106.16 + 1.46 \cdot d + 0.21 \cdot p_{inj} + 10^{-3} \cdot d \cdot p_{inj} + 1.25 \cdot 10^{-4} p_{inj}^2 \quad (7)$$

4. Conclusions

From the current state of the art, it is known that the dynamics of real liquid jets which impinge a hot wall strongly affects the surface temperature and fate of the reflected droplets after the impingement. The dynamics of the interaction may cause heavy shifts of the Leidenfrost temperature and of the Nukiyama temperature, leading to unexpected surface cooldown and liquid distribution. This effect is mainly due to the kinetic characteristics of the impinging jet, e.g. velocity magnitude, velocity direction and magnitude of the components, number density.

This work is focused on the identification of the shift of both the Leidenfrost and the Nukiyama temperature compared to the reference ones determined from the literature (experiments and correlations based on the gentle deposition of single droplets). As application area, the wall impingement of fuel sprays in internal combustion engines has been chosen because the current injection techniques (high pressure injection, full-cone sprays, small nozzle diameter) are representative of high velocity and high number density jets. The study has been conducted by means of three-dimensional CFD and one-dimensional FEM coupled simulations. The following points summarize the results of the investigation:

- the simulations can reproduce the transition boiling regime and the film boiling regime. Increasing the temperature of the surface from 298 K to 423 K causes a local cooldown of the surface of 8 K. The cooling rate is higher as the injection pressure increases. The rising the temperature up to 493 K causes the gradual reduction the local cooldown of the surface up to zero due to the occurrence of the Leidenfrost effect. Indeed, at 493 K, a consistent part of the injected mass is in the form of dispersed liquid, whilst no wall film has been recorded;
- the computed boiling curves of the test fuel show a maximum heat flux delayed compared to the expectations based on the reference Nukiyama temperature. The Nukiyama temperature is shifted upward of 8 K and 25 K for the injection pressure values 300 bar, and 700 bar, respectively;
- under real spray conditions, the switch from transition boiling regime to film boiling regime is significantly faster. According to the reference values of the Nukiyama temperature and of the Leidenfrost temperature, the switch requires to heat up the surface of 44 K. From CFD simulations it is visible that the switch happens by heating the surface of 20 K – 30 K, depending on the injection pressure and the injector-surface distance;
- depending on the operating conditions, the Leidenfrost effect can be both anticipated or delayed compared to the expectations. Under the investigate conditions, a maximum backward shift of 30 K and a maximum upward shift of 10 K have been recorded. The occurrence of anticipated or delayed Leidenfrost effect has been correlated to the distribution of the kinetic energy along the perpendicular or the parallel direction compared to the wall as well as to the injection pressure and the injector-wall distance. In the case of pump gasoline, if the Weber number of the droplets is higher than 1800, the Leidenfrost effect is delayed at any distribution of the kinetic energy between the two directions.

CRediT authorship contribution statement

Davide Viscione: Writing – original draft, Visualization, Validation, Software, Methodology, Investigation. **Valerio Mariani:** Writing – original draft, Visualization, Validation, Software, Methodology, Investigation. **Stefania Falfari:** Writing – review & editing, Supervision, Resources, Methodology. **Vittorio Ravaglioli:** Writing – review & editing, Supervision, Resources, Methodology. **Giovanni Meccariello:** Validation, Methodology, Formal analysis. **Alessandro Montanaro:** Validation, Supervision, Resources, Methodology.

Declaration of competing interest

The authors declare that they have no known competing financial interests or personal relationships that could have appeared to influence the work reported in this paper.

Funding

This research did not receive any specific grant from funding agencies in the public, commercial, or not-for-profit sectors.

Data availability

Data will be made available on request.

References

[1] A. Faghri, Y. Zhang, Transport Phenomena in Multiphase Systems, Academic Press, 2006, pp. 765–852.
[2] Y.A. Cengel, Heat Transfer: A Practical Approach, McGraw Hill, 2003, pp. 785–841.
[3] Stanglmaier, R., Roberts, C., Moses, C., Vaporization of individual fuel drops on a heated surface: a study of fuel-wall interactions within direct-injected gasoline (DIG) engines, SAE Technical Paper 2002-01-0838, 2002, doi:10.4271/2002-01-0838.
[4] T.Y. Xiong, M.C. Yuen, Evaporation of a liquid droplet on a hot plate, Int. J. Heat Mass Transf. 34 (7) (1991) 1881–1894, https://doi.org/10.1016/0017-9310(91)90162-8.
[5] R.W. Temple-Pediani, Fuel drop vaporization under pressure on a hot surface, Proc. Inst. Mech. Eng. 184 (1) (1969) 677–696, https://doi.org/10.1243/PIME_PROC_1969_184_053_02.
[6] D. Fardad, N. Ladommatos, Evaporation of hydrocarbon compounds, including gasoline and diesel fuel, on heated metal surfaces, Proc. Inst. Mech. Eng. D 213 (6) (1999) 625–645, https://doi.org/10.1243/0954407991527152.
[7] A.A. Mills, J.D. Fry, Rate of evaporation of hydrocarbons from a hot surface: nukiyama and Leidenfrost temperatures, Eur. J. Phys. 3 (152) (1982), https://doi.org/10.1088/0143-0807/3/3/005.
[8] S. Yao, K.Y. Cai, The dynamics and leidenfrost temperature of drops impacting on a hot surface at small angles, Exp. Therm. Fluid Sci. 1 (4) (1988) 363–371, https://doi.org/10.1016/0894-1777(88)90016-7.
[9] N. Garcia Rosa, P. Villedieu, et al., A new droplet-wall interaction model, in: Proceedings of the 10th International Conference on Liquid Atomization and Spray System ICLASS, 2006.
[10] Bai, C., Gosman, A.D., Development of methodology for spray impingement simulation, SAE Technical Paper 950283, 1995, doi:10.4271/950283.
[11] C. Mundo, C. Tropea, M. Sommerfeld, Numerical and experimental investigation of spray characteristics in the vicinity of a rigid Wall, Exp. Therm. Fluid Sci. 15 (3) (1997) 228–237, https://doi.org/10.1016/S0894-1777(97)00015-0.
[12] K. Ashida, T. Takahashe, et al., Spray-wall interaction model considering superheating degree of the wall surface, in: 8th International Conference on Liquid Atomization and Spray System ICLASS, 2000.

[13] E. De Renzis, V. Mariani, et al., Application of a one-dimensional fuel-oil dilution model coupled with an empirical droplet-to-film formation strategy for predicting in-cylinder oil effects in a direct injection engine, J. Phys.: Conf. Ser. (2022) 2385, https://doi.org/10.1088/1742-6596/2385/1/012063.
[14] F. Schulz, W. Samenfink, et al., Systematic LIF fuel wall film investigation, Fuel 172 (2016) 284–292, https://doi.org/10.1016/j.fuel.2016.01.017.
[15] F. Chang, H. Luo, et al., Experimental investigation of fuel adhesion from wall-impinging spray with various injection mass ratios, Exp. Therm. Fluid Sci. (2025) 163, https://doi.org/10.1016/j.expthermflusci.2024.111403.
[16] R. Xu, R. Zhang, et al., Investigation on the jet impingement cooling of steel discs using air-atomized water mist, Int. J. Heat Mass Transf. (2025) 245, https://doi.org/10.1016/j.ijheatmasstransfer.2025.126989.
[17] M. Jiang, Y. Wang, et al., Inhibiting the Leidenfrost effect above 1000°C for sustained thermal cooling, Nature 601 (2022) 568–572, https://doi.org/10.1038/s41586-021-04307-3.
[18] M. Hnizdil, J. Kominek, et al., Prediction of leidenfrost temperature in spray cooling for continuous casting and heat treatment processes, Metals 10 (11) (2020), https://doi.org/10.3390/met10111551.
[19] M. Bornhorst, O. Deutschmann, Advances and challenges of ammonia delivery by urea-water sprays in SCR systems, Prog. Energy Combust. Sci. (2021) 87, https://doi.org/10.1016/j.pecs.2021.100949.
[20] A.P. Kulkarni, T. Megaritis, L.C. Ganippa, Impact dynamics and morphology of urea-water-solution droplets impinging on a hot plate under urea-SCR relevant conditions: influence of surface tension, Fuel (2021) 298, https://doi.org/10.1016/j.fuel.2021.120671.
[21] J. Wang, H. Fu, et al., Experiment investigation on the effects of air assisted SCR spray impingement on wall temperature evolution, Energy (2020) 204, https://doi.org/10.1016/j.energy.2020.117943.
[22] C. Kuhn, D. Schweigert, et al., Single droplet impingement of urea water solution on heated porous surfaces, Int. J. Heat Mass Transf. (2021) 181, https://doi.org/10.1016/j.ijheatmasstransfer.2021.121836.
[23] C.T. Avedisian, J. Koplik, Leidenfrost boiling of methanol droplets on hot porous/ceramic surfaces, Int. J. Heat Mass Transf. 30 (1987) 379–393, https://doi.org/10.1016/0017-9310(87)90126-8.
[24] A. Chausalkar, C.M. Kweon, et al., Leidenfrost behavior in drop-wall impacts at combustor-relevant ambient pressures, Int. J. Heat Mass Transf. (2020) 153, https://doi.org/10.1016/j.ijheatmasstransfer.2020.119571.
[25] F. Kopple, D. Seboldt, et al., Experimental investigation of fuel impingement and spray-cooling on the piston of a GDI engine via instantaneous surface temperature measurements, SAE Int. J. Engines 7 (3) (2014) 1178–1194, https://doi.org/10.4271/2014-01-1447.
[26] P. Spiegler, J. Hopenfeld, et al., Onset of stable film boiling and the foam limit, Int. J. Heat Mass Transf. 6 (11) (1963) 987–989, https://doi.org/10.1016/0017-9310(63)90053-X.
[27] C. Habchi, New correlations for Leidenfrost and Nukiyama temperatures with gas pressure application to liquid film boiling simulation, in: Proceedings of the 23rd Annual Conference on Liquid Atomization and Spray Systems ILASS, 2010, https://doi.org/10.13140/2.1.1699.4242.
[28] C. Habchi, A comprehensive model for liquid film boiling in internal combustion engines, oil & gas science and technology – rev, IFP 65 (2) (2010) 331–343, https://doi.org/10.2516/ogst/2009062.
[29] D. Viscione, V. Mariani, et al., Investigation of the GCI main injection: experimental-numerical analysis of gasoline spray impact at reference engine conditions, Int. J. Multiph. Flow (2025) 182, https://doi.org/10.1016/j.ijmultiphaseflow.2024.105034.
[30] K.Y. Huh, A.D. Gosman, A phenomenological model of diesel spray atomization, in: Proceedings of the International Conference on Multiphase Flow, 1991.
[31] Reitz, R.D., Diwakar, R., Effect of drop breakup on fuel sprays, SAE Technical Paper 860469, 1986, doi:10.4271/860469.
[32] P.J. O'Rourke, Collective Drops Effects on Vaporizing Liquid Sprays, Princeton University, 1981. Ph.D. Thesis.
[33] D. Viscione, V. Mariani, et al., Unconventional gasoline spray injection events: compared evolution of experimental data and numerical simulations, Fuel (2024) 355, https://doi.org/10.1016/j.fuel.2023.129438.
[34] V. Mariani, G.M. Bianchi, et al., Fuel droplet-wall impingement under GDI-like conditions: a numerical investigation, AIP Conf. Proc. 2191 (1) (2019), https://doi.org/10.1063/1.5138840.
[35] Y. Liu, M. Monde, et al., Evaporation time and vapor generation limit of a droplet on a hot surface, Int. J. Heat Mass Transf. (2021) 173, https://doi.org/10.1016/j.ijheatmasstransfer.2021.121280.
[36] S. Hidaka, Y. Takata, et al., Wettability and droplet evaporation on plasma-irradiated metal surface, Trans. Jpn. Soc. Mech. Eng. B 69 (678) (2003) 437–444, https://doi.org/10.1299/kikaib.69.437.